Similarity Metric For Curved Shapes In Euclidean Space

Girum G. Demisse   Djamila Aouada   Björn Ottersten

Interdisciplinary Center for Security, Reliability and Trust
University of Luxembourg, 4, rue Alphonse Weicker, L-2721, Luxembourg

{girum.demisse, djamila.aouada, bjorn.ottersten}@uni.lu

Abstract

In this paper, we introduce a similarity metric for curved shapes that can be described, distinctively, by ordered points. The proposed method represents a given curve as a point in the deformation space, the direct product of rigid transformation matrices, such that the successive action of the matrices on a fixed starting point reconstructs the full curve. In general, both open and closed curves are represented in the deformation space modulo shape orientation and orientation preserving diffeomorphisms. The use of direct product Lie groups to represent curved shapes led to an explicit formula for geodesic curves and the formulation of a similarity metric between shapes by the L^2-norm on the Lie algebra. Additionally, invariance to reparametrization or estimation of point correspondence between shapes is performed as an intermediate step for computing geodesics. Furthermore, since there is no computation of differential quantities on the curves, our representation is more robust to local perturbations and needs no pre-smoothing. We compare our method with the elastic shape metric defined through the square root velocity (SRV) mapping, and other shape matching approaches.

1. Introduction

The analysis of the shape of an object has several applications in computer vision, engineering, computational anatomy, and bioinformatics [23, 14, 6]. In fact, in [16] the practical importances of shape analysis and modelling were categorized as *shape optimization*: finding a shape that satisfies a certain design requirement, e.g. active contours, and *shape analysis*: statistical analysis of shapes, e.g. distance between shapes, mean shapes and probability distribution of shapes. Consequently, a significant effort has been made to describe shapes based on features or landmarks that satisfy predefined requirements [28, 1]. However, in [24] feature based approaches are argued to be inadequate to represent a shape; since, shape space in gen-
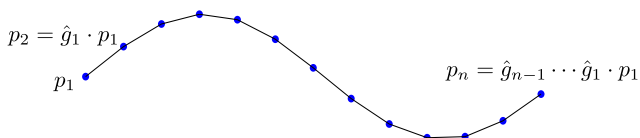

Figure 1: Illustration of the proposed representation. Given the discrete path starts at point p_1, the curve's representation is $(\hat{g}_1, \cdots, \hat{g}_{n-1})$, where the $\hat{g}$'s are rigid transformation matrices.

eral is formulated as non-linear and infinite dimensional space. Thus, theoretically, an infinite-dimensional object can not distinctively be represented by a finite-dimensional feature. For instance, landmark-based approaches [10] require the landmark points to be selected either automatically or with expert's input. This leads to inconsistent representation, as the same shape can, potentially, be represented by two completely different sets of landmark points. In contrast, in [24, 29, 11] shapes were parametrized by functions. Thus, shape space is considered in its entirety as an infinite dimensional space. Moreover, the infinite dimensional space is complemented with a distance metric. Hence, in principle, shape space is framed as infinite dimensional Riemannian manifold. There are several advantages in using the Riemannian framework to define a shape space. The first advantage is the treatment of shape space as a smooth manifold which is only natural considering the non-linearity of shapes. Secondly, the Riemannian framework offers a smoothly varying metric, which is essential to measure distance, area and other associated geometric notions in the shape space. Furthermore, under the Riemannian framework, shape space can be linearised, at least locally, without disregarding the non-linear nature of shapes; effectively, opening shape analysis problems to statistical treatment. Consequently, several and different distance metrics were considered in infinite dimensional manifolds [25, 16, 11, 17, 18, 29].

In the infinite dimensional setting, shape space is usually

given as $\text{Imm}(\mathbb{S}^1, \mathbb{R}^n)/\text{Diff}(\mathbb{S}^1)$, where $\text{Imm}(\mathbb{S}^1, \mathbb{R}^n)$ is the space of all parametrized functions immersed in $\mathbb{R}^n$ and defined on a 1-dimensional circle, $\mathbb{S}^1$, while $\text{Diff}(\mathbb{S}^1)$ is the group of diffeomorphisms acting on $\mathbb{S}^1$. The most common metric in such a space is $L^2(a, b) = \int \langle a, b \rangle \mathrm{d}s$, where a and b are vector fields tangent to a curve at the shape space and integrated with respect to the arc length. Although, this metric looks simple, its geodesic equation is difficult to solve. More ominously, the L^2 metric can potentially result in a zero distance between two different shapes [17, 16]. Consequently, to avoid such behaviour first order Sobolev metric was introduced [17], with numerical solutions. In [25], an isomorphism from $\text{Imm}(\mathbb{S}^1, \mathbb{R}^n)/\text{Diff}(\mathbb{S}^1)$, with first order Sobolev metric, to Hilbert manifold, with L^2 metric, was presented by a mapping function called *square root velocity* (SRV). As a result, the first order Sobolev metric was shown to be equivalent to L^2 metric on a Hilbert manifold for certain weighting constants. This led to a numerically efficient distance computation between shapes. Thus, in [25], geodesic paths were computed with a closed-form formula for open curves. For closed curves, however, the geodesic distance is computed with an iterative method called "path-straightening". In [19], a metric that leads to explicit geodesics of planar curves is presented. Nonetheless, in almost all parametrization approaches shapes are assumed to be C^∞(infinitely differentiable) or at least C^2, since most approaches need to compute curvature at some stage. In fact, most metrics in infinite dimensional space are defined based on differential quantities of the curve, e.g. first order Sobolev metric. This, in general, leads to representation which is sensitive to noise, making a pre-smoothing stage a necessity [15].

Alternatively, in [7] the theme of taking optimal deformation between shapes as a similarity metric was introduced. In such a setting, a given shape is similar to another if it is a small deformation away. Hence, similarity and difference between shapes is quantified by the required deformation to align them. Although, the deformations need not be low-dimensional, e.g. rigid transformation, they can be tailored to fit a particular problem. In [6], for example, a high-dimensional deformation that does not include reflection was presented to capture variability in a 3-dimensional human body shape. In [8], a general pattern theory that analyses patterns generated by geometric units (e.g. points and lines) and their relationship based on transformations that act on the units is presented. In general, the optimal deformation approach gives a similarity metric that is robust to noise or outliers unlike other differential based metrics or Hausdorff distance (L^∞), for example. However, in most cases the computation of optimal deformation is numerically intensive [29, 7, 8].

In this work, we build on [4] and formulate a new curved shape representation on the deformation space, which leads
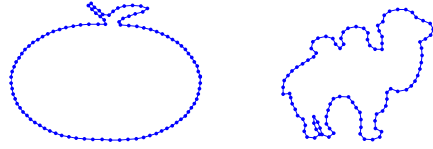

Figure 2: Examples of closed curved shapes with 100 uniformly sampled points

to a much simpler similarity metric that is equivalent to L^2-norm. The proposed approach computes the optimal deformation as a similarity metric. Nonetheless, we do not only compute optimal deformation as a metric but explicitly represent the curves in the deformation space, which, in our case, is a finite dimensional Lie group. We also do not refer to a template shape to compute deformations which is the case in [29, 7, 6, 8, 4]. To encode how a given curve is deforming through space, a curved shape is represented by finitely many rigid transformation matrices that are required to construct the whole curve from a given starting point, see Figure 1. In essence, the transformation matrices capture how the shape bends and stretches through space. The key point of the approach is in using the already established Riemannian structure of the rigid transformation matrix space to compute distance and estimate point correspondence. Overall, the main advantage of our approach is the computation of geodesic distance between shapes by L^2-norm; closed form solution for geodesic path between two shapes is possible. Furthermore, the similarity metric is relatively robust to local perturbations, and deformation of a shape can be factored with matrix manipulation. Although the proposed method is closer to [7], we will compare our results with [25], mainly because it has since been applied to a wide variety of problems.

The rest of the paper is organized as follows: in Section 2 we will formalize and discuss the proposed shape representation, definition of similarity metric and point correspondence estimation. In Section 3 experimental results of the proposed metric is reported. The paper ends with concluding remarks in Section 4.

2. Shape representation

Assume a given curved shape S is distinctively described by a set of k discrete points uniformly sampled from the boundary of the shape. In practice, this is done by enforcing a roughly equal arc length between consecutive points, see Figure 2. Subsequently, similar to [10], location and uniform scaling of a given shape, $S = (p_1, \cdots, p_k)$ where $p_i \in \mathbb{R}^n$, are filtered out as follows

$$\mathcal{S} = (p_1^*, \cdots, p_k^*) = \left(\frac{p_1 - \bar{p}}{h}, \cdots, \frac{p_k - \bar{p}}{h} \right), \quad (1)$$

where

$$\bar{p} = \frac{1}{k} \sum_i^k p_i \in \mathbb{R}^n, \quad h = \sqrt{\sum_i^k \| p_i - \bar{p} \|_2^2} \in \mathbb{R},$$

where $\| \cdot \|_2$ denotes L^2-norm. Thus, any curved shape $\mathcal{S}$ is a point in $\mathbb{R}^{kn}$. Furthermore, the sampled points are assumed to be ordered according to arc length. The starting point p_1 and ordering direction of a path are selected arbitrarily. Later in the paper, we will discuss the impact of ordering direction and selection of starting point; this is similar to what was described as reparametrization in the literature [16, 25]. We further denote the space of k ordered and normalized points, using (1), by $\mathcal{C}$. Subsequently, any curved shape $\mathcal{S}_i \in \mathcal{C}$ is assumed to be able to deform into any other shape $\mathcal{S}_j \in \mathcal{C}$ by a group action; i.e. $\alpha : G \times \mathcal{C} \rightarrow \mathcal{C}$ where G is a group. In this work, we will only consider Euclidean transformations without reflection and thus the group under consideration is the direct product of Special Euclidean group; i.e. $G = \text{SE(n)}^k$. To that end, the deformation of a shape by group action is given as $\mathcal{G}\mathcal{S} = (g_1 p_1, \cdots, g_k p_k)$, where $G \ni \mathcal{G} = (g_1, \cdots, g_k)$ such that $g_i \in \text{SE(n)}$. However, deformations that do not change the nature of the shape, e.g. rotation of a shape, are redundant and need to be filtered out. In addition, since scale and location are filtered out from $\mathcal{S}$, we can restrict shape preserving deformations to a particular subgroup $Q = \{ (q_1, q_2, \cdots, q_k) \in \text{SO(n)}^k \mid q_1 = q_2 \cdots = q_k \}$; here, SO(n) denotes the special orthogonal group. Consequently, the deformation of a given shape $\mathcal{S}_j$ by any $\mathcal{Q} \in Q$ will define an equivalence class $[\mathcal{S}_j]$ in $\mathcal{C}$. Thus, $[\mathcal{S}_j]$ is the set of all shapes that are generated by rotating $\mathcal{S}_j$. The key point of this paper, however, is in identifying a given shape $\mathcal{S} \in \mathcal{C}$ by a group element $\hat{\mathcal{G}} \in G$, using the imposed order of points. More precisely, a mapping function is defined on $\mathcal{C}$ as follows

$$f(\mathcal{S}) = \begin{cases} \hat{\mathcal{G}} = (\hat{g}_1, \cdots, \hat{g}_k) & \text{if } \mathcal{S} \text{ is a closed curve} \\ \hat{\mathcal{G}} = (\hat{g}_1, \cdots, \hat{g}_{k-1}) & \text{if } \mathcal{S} \text{ is an open curve} \end{cases}$$
$$(2)$$

such that

$$\hat{g}_i \times p_i = p_{i+1}.$$

Given a staring reference point p_1 and an ordering direction, the inverse of the mapping function, for closed curves, is defined as

$$f^{-1}(\hat{\mathcal{G}}) = (p_1, \hat{g}_1 p_1, \hat{g}_2 \hat{g}_1 p_1, \cdots, \hat{g}_k \cdots \hat{g}_1 p_1). \quad (3)$$

The inverse for open curves can be defined similar to (3). Consequently, given a fixed starting point and ordering direction, any shape $\mathcal{S} \in \mathcal{C}$ has a unique representation in G, see Appendix A on computing the optimal $g \in \text{SE(n)}$ between two high dimensional points. Intuitively, $f(\cdot)$ employs the order of points to capture how a curved shape bends and stretches along the path starting from a fixed point. More importantly, $f(\cdot)$ preserves the shape equivalence relationship induced by rotating shapes.

Proposition 1. *If $\hat{\mathcal{G}}^a$ and $\hat{\mathcal{G}}^b$ are the representations of $\mathcal{S}_a, \mathcal{S}_b \in [\mathcal{S}_j]$ then $\hat{\mathcal{G}}^a$ is equivalent to $\hat{\mathcal{G}}^b$ by conjugacy, $\hat{\mathcal{G}}^a \sim \hat{\mathcal{G}}^b$.*

Proof. Since, $\mathcal{S}_a, \mathcal{S}_b \in [\mathcal{S}_j]$ we can write $\mathcal{S}_a = \mathcal{Q}\mathcal{S}_b$ where $\mathcal{Q} = (q_1, \cdots, q_k) \in Q$. Let $\mathcal{S}_a = (p_1^a, \cdots, p_k^a)$ and $\mathcal{S}_b = (p_1^b, \cdots, p_k^b)$, then from (2) we have

$$\begin{aligned} \hat{g}_i^b \times p_i^b &= p_{i+1}^b \\ &= q_{i+1} \times p_{i+1}^a \\ &= q_{i+1} \times \hat{g}_i^a \times p_i^a \end{aligned}$$

Since $q_1 = q_2 = \cdots = q_k$, we can compute elements of $\hat{\mathcal{G}}^b$ in terms of $\hat{\mathcal{G}}^a$ as follows

$$\hat{g}_i^b \times q_i \times p_i^a = q_{i+1} \times \hat{g}_i^a \times p_i^a$$
$$\hat{g}_i^b = q_i \times \hat{g}_i^a \times q_i^{-1}.$$

Thus, $\hat{\mathcal{G}}^a$ and $\hat{\mathcal{G}}^b$ are equivalent by conjugacy, i.e., $\hat{\mathcal{G}}^b = \mathcal{Q}\hat{\mathcal{G}}^a \mathcal{Q}^{-1}$ ∎

Although the above proof is done for closed curve representations, the argument is equally valid for open curve representations as well. Furthermore, given point correspondence between any two shapes, $\mathcal{S}_a$ and $\mathcal{S}_b$, the optimal rotation $\mathcal{Q}$, such that $\mathcal{S}_a = \mathcal{Q}\mathcal{S}_b$, can be computed by optimizing the following

$$\min_{\mathcal{Q} \in Q} \| \mathcal{Q}\mathcal{S}_b - \mathcal{S}_a \|_2^2. \quad (4)$$

In such a case, $\mathcal{S}_a$ and $\mathcal{S}_b$ are in the same shape class if $f(\mathcal{S}_b) = \mathcal{Q}f(\mathcal{S}_a)\mathcal{Q}^{-1}$. Computationally, if two given shapes belong to the same shape class then the corresponding eigenvalues of the transformation matrices in $f(\mathcal{S}_b)$ and $f(\mathcal{S}_a)$ are similar.

In summary, closed and open curves are represented by elements of $\text{SE(n)}^k/Q$ and $\text{SE(n)}^{k-1}/Q$, respectively. At this stage, we are still assuming a given parametrization. Thus, neither $\text{SE(n)}^k/Q$ nor $\text{SE(n)}^{k-1}/Q$ are invariant to reparametrization; we will address this issue later on the paper. However, it must be noted that SE(n)^k is not a representation space exclusive to closed curves only–the representation space SE(n)^k can potentially include open curves described by $(k+1)$ points.

2.1. Distance in SE(n)^k

The formulated shape representation space SE(n)^k is a Lie group, thus is a non-linear space. As a result, the usual definition of shortest path as a straight line does not generalize to SE(n)^k. In this subsection, we will provide an informal definition of Lie group, overview concepts from differential geometry and define distance in SE(n) and in the product group SE(n)^k.

A Lie group is a differentiable or smooth manifold with a smooth group operations; that is, the group's binary operator $(x, y) \mapsto xy^{-1}$ is smooth. Furthermore, the tangent space at the identity element e of a Lie group is an algebra called Lie algebra. Henceforth, we will denote the tangent space of a smooth manifold M at $p \in M$ by $T_p M$, e.g. the Lie algebra of SE(n) is denoted as $T_e M$ or $\mathfrak{se}(n)$. Since a Lie group has a smooth invertible binary operator it can be anchored to any element $a \in G$ so that it defines a diffeomorphism onto itself. For instance, the left translation of a Lie group defined as $L_a : G \to aG$. However, to compute distance, volume and other geometric notions, an additional structure called metric is needed. Subsequently, a differentiable manifold M complemented with a smoothly varying metric tensor q is called a Riemannian manifold (M, q); the metric tensor q is defined at the tangent space $T_p M$ as $q_p : T_p M \times T_p M \to \mathbb{R}^{\geq 0}$ for every $p \in M$, see [21, 5]. As a result, the distance between $A, B \in M$ is defined as

$$d(A, B) = \text{Inf}\{\int_a^b \sqrt{\dot{\gamma}(t)^T q_t \dot{\gamma}(t)} \mathrm{d}t\}, \qquad (5)$$

where $\dot{\gamma}(\cdot)$ is the derivative of any curve defined on a subset of $\mathbb{R}$, $\gamma : [a, b] \to M$ such that $\gamma(a) = A$ and $\gamma(b) = B$. Although, there are many curves that start at A and end at B the one that satisfies (5) is called geodesic curve.

A Riemannian metric on a Lie group is said to be left translation invariant if the left translation diffeomorphism is an isometery, i.e., if the following is true

$$\langle x, y \rangle_e = \langle dL_a x, dL_a y \rangle_a, \quad \forall x, y \in T_e M, \forall a \in G, \quad (6)$$

where dL_a is the derivative of the left translation. In such a case, a left translation invariant Riemannian metric is identified with scalar product $\langle \cdot, \cdot \rangle$ defined on the Lie algebra, $\mathfrak{se}(n)$, through the pullback map, dL_a^{-1}. More interestingly, if a vector field $\dot{\gamma}$ on a Lie group is left translation invariant, i.e., if the following is true for $\dot{\gamma}(h) \in T_h M$

$$dL_a \dot{\gamma}(h) = \dot{\gamma}(ah) \in T_{ah} M, \qquad (7)$$

then its integral curve $\gamma(t) = \exp(t\dot{\gamma})$ is geodesic. In a similar argument, a geodesic curve in SO(n) and $\mathbb{R}^n$ can be defined, respectively, as follows

$$\beta(t) = R_1 (R_1^{-1} R_2)^t \qquad (8)$$
$$\alpha(t) = v_1 + (v_2 - v_1)t, \qquad (9)$$

where $t \in [0, 1]$. It can easily be checked that $\beta(\cdot)$ is geodesic in SO(n), though, not necessarily unique [20, 2], whereas $\alpha(\cdot)$ is clearly geodesic since $\mathbb{R}^n$ is a vector space. Meanwhile, SE(n), which is not a compact group, is a semi-direct product of a compact group, SO(n), and $\mathbb{R}^n$; it can be represented in homogeneous coordinates as follows

$$g_i = \begin{pmatrix} R_i & v_i \\ 0 & 1 \end{pmatrix}, \text{ s.t., } R_i \in \text{SO(n)}, \ v_i \in \mathbb{R}^n. \qquad (10)$$

Consequently, in [30] the following curve in SE(n) is proven to be geodesic.

$$\varphi(t) = \begin{pmatrix} R_1 (R_1^{-1} R_2)^t & v_1 + (v_2 - v_1)t \\ 0 & 1 \end{pmatrix}, \qquad (11)$$

where $t \in [0, 1]$. Subsequently, we can define a scalar product on the Lie algebra as

$$\langle (\mathfrak{R}_1, v_1), (\mathfrak{R}_2, v_2) \rangle = \langle \mathfrak{R}_1, \mathfrak{R}_2 \rangle + \langle v_1, v_2 \rangle, \qquad (12)$$

where, $\mathfrak{R} \in \mathfrak{so}(n)$, is the Lie algebra of SO(n). Thus, the length of a geodesic curve connecting $g_1, g_2 \in$ SE(n) can be computed by transporting the tangent vectors with the pullback to the Lie algebra. The geodesic distance, in this case, reads as

$$d(g_1, g_2) = \int_0^1 \langle dL_{\varphi(t)}^{-1}(\dot{\varphi}(t)), dL_{\varphi(t)}^{-1}(\dot{\varphi}(t)) \rangle \mathrm{d}t, \qquad (13)$$

where $\langle \cdot, \cdot \rangle$ is as defined in (12). Since $\varphi(t)$ is a geodesic curve, the tangent vectors $\dot{\varphi}(t)$ are parallel along $\varphi(t)$. Hence, the geodesic distance given in (13) is reduced to the following

$$d(g_1, g_2) = (\| \log(R_1^T R_2) \|_F^2 + \| v_2 - v_1 \|_2^2)^{1/2}, \qquad (14)$$

where $\| \cdot \|_F$ denotes the Frobenius norm. At this stage, we can extend the geodesic curve (11) to the direct product space SE(n)^k = SE(n)$_1 \times \cdots \times$ SE(n)$_k$ as follows

$$\zeta(\hat{\mathcal{G}}_A, \hat{\mathcal{G}}_B) = (\varphi(t)_1, \cdots, \varphi(t)_k), \qquad (15)$$

such that $\varphi(t)_i$ is the geodesic curve between $g_i \in \hat{\mathcal{G}}_A$ and $g_i \in \hat{\mathcal{G}}_B$. It can be shown that (15) is a geodesic curve in the product group, see [5]. Subsequently, we can define the distance in SE(n)^k, using the product metric, as follows

$$\mathfrak{d}(\hat{\mathcal{G}}_A, \hat{\mathcal{G}}_B) = (d(\hat{g}_A^1, \hat{g}_B^1)^2 + \cdots + d(\hat{g}_A^k, \hat{g}_B^k)^2)^{1/2}. \qquad (16)$$

In effect, the geodesic path and distance between two shapes $\mathcal{S}_A, \mathcal{S}_B \in \mathcal{C}$, represented by $\hat{\mathcal{G}}_A$ and $\hat{\mathcal{G}}_A$, respectively, can be computed using (15) and (16), see Alg. 1, Alg. 2 and Figure 3. We again stress that (16) is subject to point correspondence or parametrization.
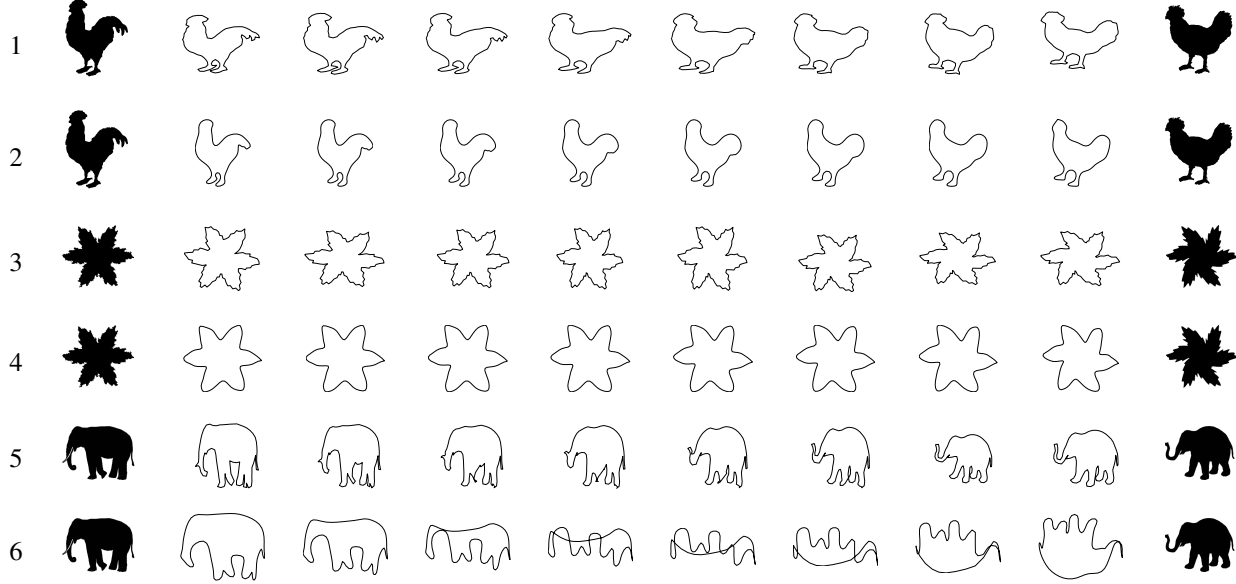
Figure 3: Shapes along the geodesic path between the first and the last shape which are the original input shapes. The odd rows show results from our approach while the even row are results from [25]. All shapes are represented by 100 uniformly sampled and normalized points. We note that results from [25] are smoothed and lost local features of the shape.

Algorithm 1: Geodesic distance between closed curves

Data: $\{\hat{g}_A^1 \cdots \hat{g}_A^k\}, \{\hat{g}_B^1 \cdots \hat{g}_B^k\} \in \text{SE(n)}^k$
Initalization: $i = 1, \mathfrak{d} = 0$;
for $i \leq k$ **do**
$\quad d(\hat{g}_A^i, \hat{g}_B^i) = \|\log((R_A^i)^T R_B^i)\|_F^2 + \|v_B^i - v_A^i\|_2^2$;
$\quad \mathfrak{d} = \mathfrak{d} + d(\hat{g}_A^i, \hat{g}_B^i); i = i + 1$;
end
Result: $\mathfrak{d} = (\mathfrak{d})^{1/2}$

Algorithm 2: Geodesic curve between closed curves

Data: $\hat{\mathcal{G}}_0 = \{\hat{g}_0^1 \cdots \hat{g}_0^k\}, \hat{\mathcal{G}}_1 = \{\hat{g}_1^1 \cdots \hat{g}_1^k\} \in \text{SE(n)}^k$
Initalization: $i = 1, N = \#steps, j = \frac{1}{N+1}$;
for $j \leq \frac{N}{N+1}$ **do**
$\quad$ **for** $i \leq k$ **do**
$\quad\quad \hat{g}_j^i = \begin{pmatrix} R_0^i((R_0^i)^{-1}R_1^i)^j & v_0^i + (v_1^i - v_0^i)j \\ 0 & 1 \end{pmatrix}$;
$\quad\quad i = i + 1$;
$\quad$ **end**
$\quad j = j + \frac{1}{N+1}$;
end
Result: $\{\hat{\mathcal{G}}_{1/N+1}, \cdots, \hat{\mathcal{G}}_{N/N+1}\}$

2.2. Properties of the metric

The proposed metric does not compute differential quantities of curved shapes. On the contrary, most infinite-dimensional representations compute differentials of the curve to define similarity metrics [25, 16]. Differentials, especially higher derivatives, are highly sensitive to noise and local perturbations. As a result, differential based approaches pre-smooth the input curves before processing it while incurring loss of potentially informative data. For instance, legitimate features due to local perturbation will be washed out because of the pre-smoothing procedure, see Figure 3, row 2, 4 and 6. Although our representation is based on the relative transformation matrices between neighbouring points, it is not as severely sensitive as curvature is, for example, to local perturbations [15].

Moreover, the proposed metric is a left translation invariant metric. Thus, the distance between two shapes remains the same even under a deformation acting on both shapes. For instance, if $\mathcal{G}_1 \in \text{SE(n)}^k$ is a deformation acting on shape S_A and S_B then, $\mathfrak{d}(\hat{\mathcal{G}}_A, \hat{\mathcal{G}}_B) = \mathfrak{d}(\mathcal{G}_1 \cdot \hat{\mathcal{G}}_A, \mathcal{G}_1 \cdot \hat{\mathcal{G}}_B)$. This fact can be observed by plugging the action of $\mathcal{G}_1$ into (14) in which case it will cancel itself out. This property is particularly important in transporting deformation between two similar shapes.

In [25], deformation transportation was framed as follows: Let S_1 and S_1' be shape contours representing exactly the same real world object O_1, only S_1' is deformed under external force, e.g., different viewing angle. And let O_2 be a similar object to O_1, but not identical, with S_2 as its shape contour. Transporting deformation is then framed as estimating how S_2 will deform, under the same external force, to give S_2'. In our framework, the deformation due to the
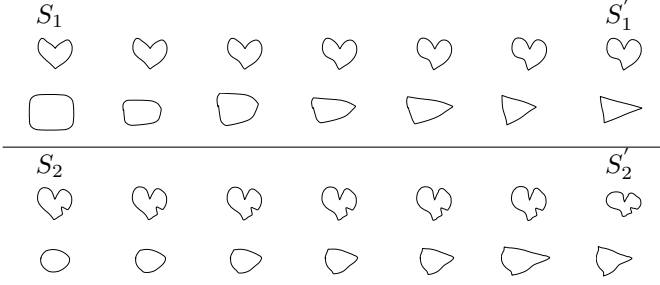
Figure 4: The first set of shapes shows two examples where S_1 deforms to S_1' due to some unknown external factor. The second set shows the transported deformation to their similar objects S_2 to give S_2', respectively.

external force can be factored out as $G_1 \cdot f(S_1) = f(S_1')$, where $f(\cdot)$ is as defined in (2). Consequently, $G_1 = f(S_1') \cdot f(S_1)^{-1}$. Since our metric is left translation invariant, $\mathfrak{d}(f(S_1), f(S_2)) = \mathfrak{d}(G_1 \cdot f(S_1), G_1 \cdot f(S_2))$. Thus, $S_2' = G_1 \cdot f(S_2)$, see Figure 4.

2.3. Point correspondence

As pointed out earlier, the distance function given in (16) is dependent on parametrization; it assumes point correspondence between two curved shapes. In this subsection, we will present a distance function that is invariant to reparametrization; we estimate corresponding points between two given shapes.

Given two closed curves $\mathcal{S}_A$ and $\mathcal{S}_B$ represented by k points, the estimation of point correspondence is formulated as estimating the starting point and ordering direction of the points in $\mathcal{S}_B$ such that (16) is minimized. In that regard, let ξ^i be a *k-cyclic* permutation; i.e. $\xi^i : \mathcal{S}_B \ni p_j \to p_{(i+j) \bmod k} \in \mathcal{S}_B$, where mod represents the modulo operation. Then, by construction $f \circ \xi^i = \xi^i \circ f$, where f is as defined in (2) and $\circ$ is used to denote function composition. Subsequently, for a fixed ordering direction the optimal staring point of a closed curve is given by the starting point of $\xi^i(\mathcal{S}_B)$ such that $\xi^i(\mathcal{S}_B)$ is the ordering that minimizes the following objective function

$$\mathcal{I}(f(\mathcal{S}_A), f(\mathcal{S}_B)) = \min_{i \in [1,k]} \mathfrak{d}(f(\mathcal{S}_A), \xi^i(f(\mathcal{S}_B))). \quad (17)$$

To work with ordering direction, we introduce a notation for a representation of a given shape ordered in clockwise direction and representation of the same shape ordered in anti-clockwise as $f(\overrightarrow{\mathcal{S}})$ and $f(\overleftarrow{\mathcal{S}})$, respectively. Moreover, we note that if $f(\overrightarrow{\mathcal{S}}) = (\hat{g}_1, \cdots, \hat{g}_k)$ then $f(\overleftarrow{\mathcal{S}}) = (\hat{g}_k^{-1}, \cdots, \hat{g}_1^{-1})$. In light of the direction notation, the optimal starting point and ordering direction of $\mathcal{S}_B$ with respect to $\mathcal{S}_A$ is given by the solution of the following

$$\min(\mathcal{I}(f(\mathcal{S}_A), f(\overrightarrow{\mathcal{S}_B})), \mathcal{I}(f(\mathcal{S}_A), f(\overleftarrow{\mathcal{S}_B}))). \quad (18)$$
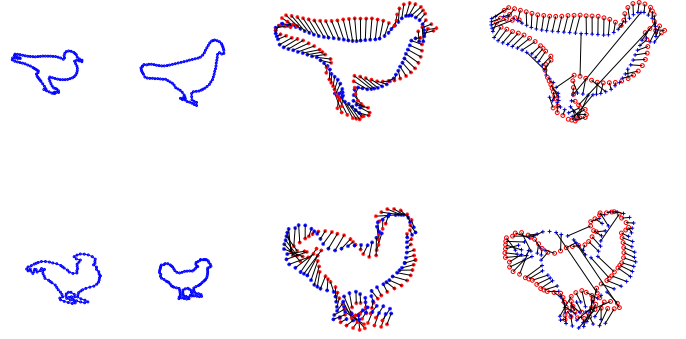

Figure 5: The first and the second columns show the input shapes for correspondence point estimation. The third column shows the estimated corresponding points with our methods and the last column are results estimated with Shape Context [1]. For visual clarity, we have scaled the results.

In effect, equation (18) is presented as the distance between two closed curves $\mathcal{S}_A$ and $\mathcal{S}_B$ where point correspondence is not known a priori. Evidently, (18) can also be used for finding correspondence between two closed curves, see Figure 5. The corresponding points between two open curve can be computed by dropping the *k-cyclic* permutation and optimizing the ordering direction alone. The solution of (18) is estimated with a brute-force approach using a nested loop iteration. Thus, the time-complexity for closed curves is $\mathcal{O}(k^2)$. More concretely, on Intel core i7-3540M with 3.0 GHz×4 processing speed and 7.7 GB RAM running Ubuntu 14.04 64-bit, MATLAB implementation of the proposed metric, given in (16), took 0.0868 seconds, and the whole distance computation set-up, including point-correspondence estimation and shape representation, took 11.0509 seconds for shapes approximated by $k = 100$ points.

In summary, the proposed point-correspondence estimation technique assumes the sampling of points with equal arclength spacing. In such cases, the approach performs with a reasonable accuracy. On the contrary, for cases where a significant warping is required due to high variation in curvature, for example, accuracy degrades. Furthermore, the proposed approach does not consider occlusion.

3. Experiments

In this section we report experimental results of the proposed similarity metric on plant leaf classification problem. Furthermore, experimental results on the robustness of the metric to local shape perturbations is provided.

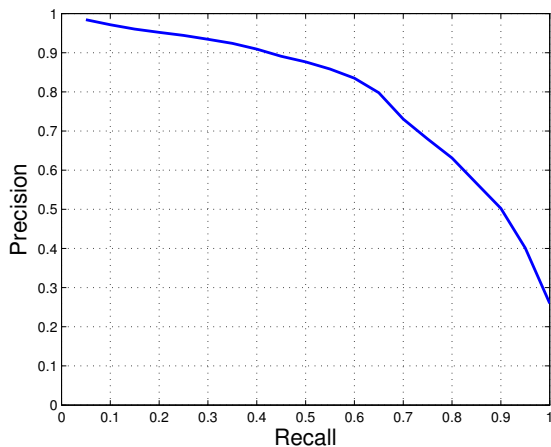Figure 7: Examples of different leaf types from the Flavia dataset.

Figure 6: Precision-recall curve of our metric on the Flavia dataset. In [12], the precision-recall curve of several approaches is presented.

3.1. Plant leaf classification

Plant leaves are traditionally classified by experts [3]. However, the magnitude of the data that is being collected is growing exponentially, rendering manual labeling inefficient. To address this problem, several feature based and shape analysis methods were proposed [12, 13, 3]. Although, color and texture are valuable features, shape is the most discriminative, as it is rarely affected by season and environmental conditions [12]. Consequently, we evaluate our shape based similarity metric on Flavia dataset [27]. The dataset contains 32 types of leaf species with a total of 1907 examples, see Figure 7. In [12], a leave-one-out test scenario was performed on Flavia dataset to evaluate the elastic similarity metric, derived from SRV-framework, and to compare with other approaches. Leave-one-out is a setup where every leaf is used as a query against the rest of the database. To compare our approach with other methods, we replicate the leave-one-out scenario with Mean Average Precision (MAP) used as a performance measure. For this experiment, every leaf shape is represented by $k = 200$ points that are uniformly sampled from the boundary of the shape. Table 1 summarizes the result of our approach and results reported in [12] and [22]. Although our method achieved a high MAP it is not necessarily inclusive of all the

Methods	MAP
Angle function [11]	45.87
Shape context [1]	47.00
TSLA [22]	69.93
Elastic metric with 200 points [12]	81.86
Gaussian elastic metric with 200 points [12]	92.37
Our method with 200 points	**94.11**

Table 1: Mean average precision on the Flavia dataset. We highlight the result of our approach at the bottom.

relevant information; precision drops as recall goes to 1, see Figure 6. Nonetheless, it outperformed elastic shape metric and Gaussian elastic metric, discussed in [12], in terms of MAP. One possible reason for this is that we do not pre-smooth the data and thus local details are more likely to be captured with our method.

3.2. Local shape perturbations

To demonstrate the impact of local perturbation on our metric, we test the proposed method on fighter jets dataset [26]. The dataset contains 7 types of fighter jets each with 30 examples, see Figure 9. Variation between the same type of planes is introduced by deforming parts of the plane and by the action of rotation matrices. We will begin our experiment by perturbing the shapes of the fighter jets with a noise sampled from a zero mean Gaussian distribution with different values for the standard deviation σ. For all subsequent experiments, the contour of every shape is approximated by uniformly sampled $k = 200$ points. Next, we repeat the leave-one-out test scenario where the unperturbed/original dataset is queried by every shape from the original dataset and from the datasets corrupted by a noise sampled from different Gaussian distributions. Table 2 summarizes the computed MAP values and Figure 8 shows their respective precision-recall curve. In general, we note that the proposed metric is not invariant to shape altering local perturbations, in terms of noise magnitude, it is however relatively robust to perturbations that do not alter the shape significantly, see Figure 9.

4. Conclusion

We proposed a similarity metric for closed and open curves that can be computed in a closed form solution. The
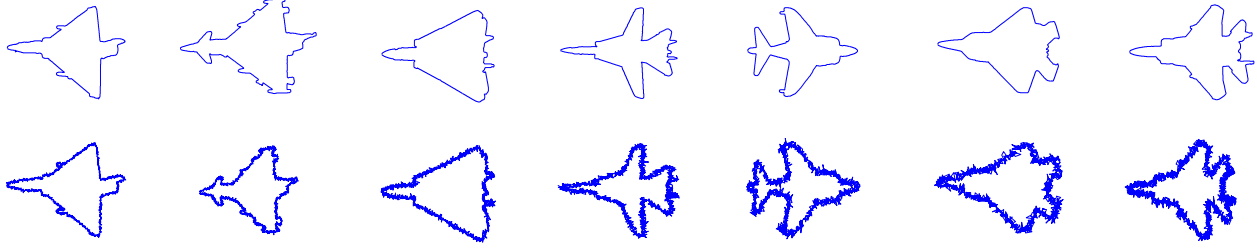
Figure 9: The first row shows the 7 types of fighter jets from [26]. The second row shows shapes with additive Gaussian noise with standard deviation of 2.5.

Noise standard deviation (σ)	MAP
0	97.11
0.5	96.72
1.5	89.95
2.5	83.27

Table 2: Mean average precision (MAP) on the fighter jets dataset for different levels of Gaussian noise.
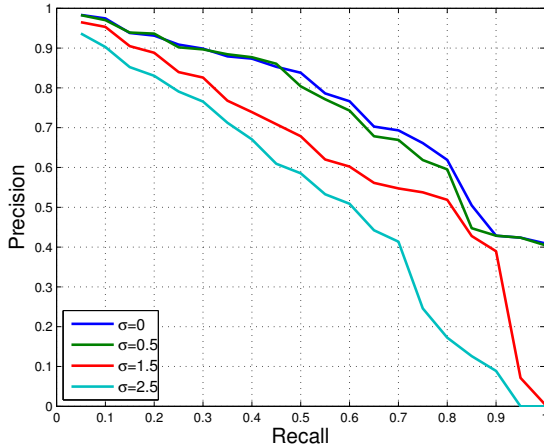

Figure 8: Precision-recall curve of our metric on the perturbed and original fighter jet planes.

key point in our metric definition is the representation of how a given curve bends and stretches with rigid transformation matrices. Subsequently, a dot product defined on the product Lie algebra is used to compute the distance between two given shapes. Following the distance metric, point correspondence estimation is given by fixing one shape and optimally ordering points of another in such a way that distance between the shapes is minimized. The proposed metric is reasonably robust to small local shape perturbations unlike metrics based on differential quantities. There are several ways one can extend the proposed metric. First, it

can be used for image retrieval systems in conjugation with other features like color and texture. Second, the dot product defined in (12) assigns the same weighing constants for the rotation (bending) and translation (stretching) quantities of the curve. This is not a necessary condition; a problem specific similarity metric that emphasizes one over the other can be defined by weighing the two terms in (14) differently. Lastly, in scenarios where a labeled training dataset is available, a label specific similarity metric can be defined by taking the covariance matrix of the label's dataset as a metric tensor to define the dot product in the Lie algebra; in (12) the metric tensor is identity.

A. Optimal transformation

The optimal rotation matrix between two vectors $p_1, p_2 \in \mathbb{R}^2$ can be computed by minimizing

$$\min_{R \in SO(2)} \|Rp_1 - p_2\|_2^2. \tag{19}$$

The solution of (19) is given as $R = VU^T$ such that the covariance of the points is $C = p_1^T p_2 = U\Sigma V^T$. However, the solution might include reflection and needs to be rectified, see [9]. Nevertheless, rotation in 2-dimensional space is about a point and similar with coordinate re-orientation. In high dimensional space this is not the case. As a result, (19) does not necessarily give a high-dimensional rotation matrix that preserves the coordinate orientation. Meanwhile, the proposed representation computes the rotations to capture the bending of a curve relative to a fixed frame. Hence, orientation preserving rotation matrix is computed by first estimating an orthonormal basis B of the space from p_1 and p_2 with SVD. Next, the rotation plane is identified as the plane on which p_1 and p_2 lie. Subsequently, R is computed by minimizing (19) and expressed in homogeneous coordinates. Finally, the rotation matrix that preserves coordinate orientation is given by $\mathcal{R} = BRB^T$.

Acknowledgment

References

[1] S. Belongie, J. Malik, and J. Puzicha. Shape matching and object recognition using shape contexts. *Pattern Analysis and Machine Intelligence, IEEE Transactions on*, 24(4):509–522, 2002.

[2] R. Bhatia. *Positive definite matrices*. Princeton University Press, 2009.

[3] J. S. Cope, D. Corney, J. Y. Clark, P. Remagnino, and P. Wilkin. Plant species identification using digital morphometrics: A review. *Expert Systems with Applications*, 39(8):7562–7573, 2012.

[4] G. Demisse, D. Aouada, and B. Ottersten. Template-based statistical shape modelling on deformation space. In *22nd IEEE International Conference on Image Processing*, 2015.

[5] M. P. do Carmo Valero. *Riemannian geometry*. 1992.

[6] O. Freifeld and M. J. Black. Lie bodies: A manifold representation of 3d human shape. In *Computer Vision–ECCV 2012*, pages 1–14. Springer, 2012.

[7] U. Grenander and D. M. Keenan. On the shape of plane images. *SIAM Journal on Applied Mathematics*, 53(4):1072–1094, 1993.

[8] U. Grenander and M. I. Miller. Representations of knowledge in complex systems. *Journal of the Royal Statistical Society. Series B (Methodological)*, pages 549–603, 1994.

[9] W. Kabsch. A solution for the best rotation to relate two sets of vectors. *Acta Crystallographica Section A: Crystal Physics, Diffraction, Theoretical and General Crystallography*, 32(5):922–923, 1976.

[10] D. G. Kendall. Shape manifolds, procrustean metrics, and complex projective spaces. *Bulletin of the London Mathematical Society*, 16(2):81–121, 1984.

[11] E. Klassen, A. Srivastava, W. Mio, and S. H. Joshi. Analysis of planar shapes using geodesic paths on shape spaces. *Pattern Analysis and Machine Intelligence, IEEE Transactions on*, 26(3):372–383, 2004.

[12] H. Laga, S. Kurtek, A. Srivastava, and S. J. Miklavcic. Landmark-free statistical analysis of the shape of plant leaves. *Journal of theoretical biology*, 363:41–52, 2014.

[13] H. Ling and D. W. Jacobs. Shape classification using the inner-distance. *Pattern Analysis and Machine Intelligence, IEEE Transactions on*, 29(2):286–299, 2007.

[14] W. Liu, A. Srivastava, and J. Zhang. Protein structure alignment using elastic shape analysis. In *Proceedings of the First ACM International Conference on Bioinformatics and Computational Biology*, pages 62–70. ACM, 2010.

[15] S. Manay, D. Cremers, B.-W. Hong, A. J. Yezzi, and S. Soatto. Integral invariants for shape matching. *Pattern Analysis and Machine Intelligence, IEEE Transactions on*, 28(10):1602–1618, 2006.

[16] A. C. Mennucci. Metrics of curves in shape optimization and analysis. In *Level Set and PDE Based Reconstruction Methods in Imaging*, pages 205–319. Springer, 2013.

[17] P. W. Michor and D. Mumford. Riemannian geometries on spaces of plane curves. *arXiv preprint math/0312384*, 2003.

[18] P. W. Michor and D. Mumford. An overview of the riemannian metrics on spaces of curves using the hamiltonian approach. *Applied and Computational Harmonic Analysis*, 23(1):74–113, 2007.

[19] P. W. Michor, D. Mumford, J. Shah, and L. Younes. A metric on shape space with explicit geodesics. *arXiv preprint arXiv:0706.4299*, 2007.

[20] M. Moakher. Means and averaging in the group of rotations. *SIAM journal on matrix analysis and applications*, 24(1):1–16, 2002.

[21] F. Morgan and J. F. Bredt. *Riemannian geometry: a beginner's guide*. Jones and Bartlett, 1993.

[22] S. Mouine, I. Yahiaoui, and A. Verroust-Blondet. A shape-based approach for leaf classification using multiscaletriangular representation. In *Proceedings of the 3rd ACM conference on International conference on multimedia retrieval*, pages 127–134. ACM, 2013.

[23] X. Pennec. Statistical computing on manifolds: from riemannian geometry to computational anatomy. In *Emerging Trends in Visual Computing*, pages 347–386. Springer, 2009.

[24] E. Sharon and D. Mumford. 2d-shape analysis using conformal mapping. *International Journal of Computer Vision*, 70(1):55–75, 2006.

[25] A. Srivastava, E. Klassen, S. H. Joshi, and I. H. Jermyn. Shape analysis of elastic curves in euclidean spaces. *Pattern Analysis and Machine Intelligence, IEEE Transactions on*, 33(7):1415–1428, 2011.

[26] N. Thakoor, J. Gao, and S. Jung. Hidden markov model-based weighted likelihood discriminant for 2-d shape classification. *Image Processing, IEEE Transactions on*, 16(11):2707–2719, 2007.

[27] S. G. Wu, F. S. Bao, E. Y. Xu, Y.-X. Wang, Y.-F. Chang, and Q.-L. Xiang. A leaf recognition algorithm for plant classification using probabilistic neural network. In *Signal Processing and Information Technology, 2007 IEEE International Symposium on*, pages 11–16. IEEE, 2007.

[28] M. Yang, K. Kpalma, J. Ronsin, et al. A survey of shape feature extraction techniques. *Pattern recognition*, pages 43–90, 2008.

[29] L. Younes. Computable elastic distances between shapes. *SIAM Journal on Applied Mathematics*, 58(2):565–586, 1998.

[30] M. Zefran, V. Kumar, and C. B. Croke. On the generation of smooth three-dimensional rigid body motions. *Robotics and Automation, IEEE Transactions on*, 14(4):576–589, 1998.